JCTC Journal of Chemical Theory and Computation

Article

pubs.acs.org/JCTC

Accurate Prediction of Essential Fundamental Properties for Semiconductors Used in Solar-Energy Conversion Devices from Range-Separated Hybrid Density Functional Theory

Moussab Harb*

Division of Physical Sciences and Engineering, KAUST Catalysis Center (KCC), King Abdullah University of Science and Technology (KAUST), 4700 KAUST, Thuwal, Makkah 23955-6900, Kingdom of Saudi Arabia

ABSTRACT: An essential issue in developing new semiconductors for photovoltaics devices is to design materials with appropriate fundamental parameters related to the light absorption, photogenerated exciton dissociation, and charge carrier diffusion. These phenomena are governed by intrinsic properties of the semiconductor like the bandgap, the dielectric constant, the charge carrier effective masses, and the exciton binding energy. We present here the results of a systematic theoretical study on the fundamental properties of a series of selected semiconductors widely used in inorganic photovoltaic and dye-sensitized solar cells such as Si, Ge, CdS, CdSe, CdTe, and GaAs. These intrinsic properties were computed in the framework of the density functional theory (DFT) along with the standard PBE and the range-separated hybrid (HSE06) exchange-correlation functionals. Our calculations clearly show that the computed values using HSE06 reproduce with high accuracy the experimental data. The evaluation and accurate prediction of these key properties using HSE06 open nice perspectives for *in silico* design of new suitable candidate materials for solar energy conversion applications.

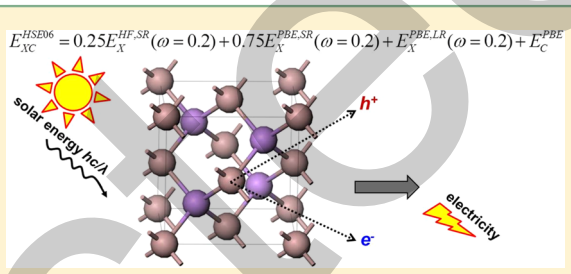

1. INTRODUCTION

Developing new semiconductor-based electronic devices for harvesting solar energy into electricity represent a grand opportunity at low environmental and economic costs.[1−5] Besides the high crystallinity needed for the developed material, the design of a suitable semiconductor for achieving efficient solar energy conversion requires three challenging fundamental parameters to be satisfied: (1) the bandgap energy should be in the 1.1−1.4 eV range to reach the optimum zone known for a maximum efficiency;[6] (2) the dielectric constant should be higher than 10 and the exciton binding energy should be lower than 25 meV (thermal energy at room temperature) to obtain an efficient dissociation of the photogenerated exciton into free charge carriers;[7−12] (3) the charge carrier effective masses should be smaller than $0.5m_0$ (m_0 is the free electron mass), at least in one crystallographic direction, to obtain good charge carrier transport properties.[7,13,14]

Modern density functional theory (DFT) is considered nowadays as an extremely valuable tool which can greatly help the experimentalists for developing a rational design of new suitable semiconducting materials for solar energy applications by computing these fundamental properties, because some of them are quite difficult to be obtained experimentally. Achieving very accurate DFT calculations, as highly required here, is directly linked to the quality of the functional used to describe the different electronic exchange and correlation interactions.

Previously, we have shown in recent theoretical studies reported on the electronic structure and UV−visible optical absorption properties of metal oxide-, oxynitride-, and nitride-based semiconductors,[15−24] that the use of DFT and density functional perturbation theory (DFPT) along with the range-separated hybrid Heyd-Scuseria-Ernzerhof (HSE06) exchange-correlation functional leads to much more accurate bandgap and optical transition predictions than those obtained from standard DFT calculations when compared to experimental data.

Our theoretical results obtained in these studies motivated us to carry out a detailed DFT study on the essential fundamental properties for solar energy conversion of a series of selected semiconductors widely used in inorganic photovoltaic and dye-sensitized solar cells such as Si, Ge, CdS, CdSe, CdTe, and GaAs. In this paper, we report the bandgaps, dielectric constant tensors, charge carrier effective mass tensors, and exciton binding energy of these materials computed using DFT employing the standard PBE and the range-separated hybrid HSE06 exchange-correlation functionals. We systematically compared our calculated values using the two functionals (PBE and HSE06) with those obtained experimentally for these semiconductors in order to define the most accurate first-principles quantum approach to be used for predicting new suitable candidate materials for solar energy conversion applications.

The rest of this paper is organized as follows. In section 2, we describe the computational details for electronic structure calculations and theoretical framework for calculations of the dielectric constant and other optical properties such as charge

Received: November 11, 2015

DOI: 10.1021/acs.jctc.5b01076
J. Chem. Theory Comput. XXXX, XXX, XXX−XXX

carrier effective masses and exciton binding energy. The calculated results are presented and discussed in section 3. Finally, we provide detailed concluding remarks in section 4.

2. COMPUTATIONAL METHODS

The crystal structures of the various studied materials were fully optimized using the periodic DFT implemented in the Vienna Ab-Initio Software Package (VASP) program,[25−28] with project-augmented plane wave (PAW) pseudopotentials.[29] Generalized gradient approximation (GGA) in the formulation of Perdew−Burke−Ernzerhof (PBE) and range-separation hybrid approximation in the formulation of Heyd-Scuseria-Ernzerhof (HSE06) were employed for the exchange-correlation functionals.[30,31] The valence atomic configurations used in the calculations were $3s^23p^2$ for Si, $4s^24p^2$ for Ge, $5s^24d^{10}$ for Cd, $3s^23s^4$ for S, $4s^24p^4$ for Se, $5s^24p^4$ for Te, $4s^24p^1$ for Ga, and $4s^24p^3$ for As. Integrations over the Brillouin zone were performed using a 5 × 5 × 5 Monkhorst−Pack k-point grid[32] for Si, Ge, CdTe, and GaAs and with a 7 × 7 × 5 k-point mesh for CdS and CdSe. The tetrahedron method with Blöchl corrections was used for the Brillouin zone integration. The plane-wave basis-set expansion was used with a kinetic energy cutoff E_{ncut} of E_{nmax}*1.33, where E_{nmax} is the recommended cutoff value for the PAW method. Values of 245.3 eV for Si, 173.8 eV for Ge, 274.3 eV for CdS, CdSe, and CdTe together with 208.7 eV for GaAs were used in our calculations for E_{nmax}. All the atomic positions and the lattice constants were relaxed until the values of the Hellman-Feynman forces were less than 0.01 eV/Å. The energy convergence criterion for the self-consistent field cycles was fixed at 10^{-6} eV. The PBE and HSE06 optimized unit-cell parameters of Si, Ge, CdS, CdSe, CdTe, and GaAs crystals as well as the corresponding experimental data are reported in Table 1. Our PBE and HSE06 calculated lattice constants are very similar, and both show values in excellent agreement with the experimental data with very small percentage errors going from 0% up to 1% using PBE and from 0% up to 1.5% using HSE06.

Table 1. Optimized Unit-Cell Parameters (in Å) for Si, Ge, CdS, CdSe, CdTe, and GaAs Crystals Computed Using PBE and HSE06 Functionals[a]

solid	structure		PBE	HSE06	expt
Si	diamond	a	5.44 (0.2%)	5.43 (0%)	5.43[7]
Ge	diamond	a	5.68 (0.3%)	5.70 (0.7%)	5.66[7]
CdS	wurtzite	a	4.13 (0%)	4.17 (0.9%)	4.13[7]
		c	6.75 (0.1%)	6.77 (0.4%)	6.74[7]
CdSe	wurtzite	a	4.33 (0.6%)	4.34 (0.9%)	4.30[7]
		c	7.09 (1%)	7.08 (0.9%)	7.01[7]
CdTe	zincblende	a	6.54 (1%)	6.56 (1.5%)	6.46[7]
GaAs	zincblende	a	5.70 (0.8%)	5.69 (0.7%)	5.65[13]

[a] a for the cubic structures; a and c for the noncubic structures. The percentage errors compared to experimental data[7,13] are given in parentheses.

The electronic bandgap and k-space band structure of each material were computed by employing the standard PBE and the range-separated hybrid HSE06 exchange-correlation functionals implemented in the VASP program, based on the optimized geometries obtained at the PBE and HSE06 levels, respectively. Note that in the HSE06 formalism, a range separation approach is taken for the exchange part, while the correlation part is defined by PBE. The range-separation parameter was fixed at 0.2 Å. At long-range interaction, the standard PBE exchange is maintained, whereas a mixing of 25% of exact Hartree−Fock (HF) and 75% of PBE exchange is used at short-range interaction. To determine the influence of relativistic effects on the computed bandgap of each solid, a single calculation was performed with VASP by taking into account the addition of spin−orbit coupling to the Hamiltonian along with the noncollinear formalism and the two PBE and HSE06 functionals.

The electronic contribution to the static dielectric constant tensor (ε_∞) of each compound was computed using the self-consistent response of the crystal to a finite external electric field[33] implemented in the VASP program along with the PBE and HSE06 functionals. This method is perturbative, which includes the local field effects and focuses on the description of the relaxation of crystalline orbitals under the effect of an external static electric field. The perturbed wave function is then used to calculate the dielectric properties as energy derivatives. This dielectric constant represents the ability of a dielectric material to screen the external electric field by the apparition of the electronic polarization induced by the electron density distortion. A good description of the bandgap generally leads to a good description of ε_∞.

The vibrational contribution to the dielectric constant (ε_{vib}) was obtained by computing the full phonon spectrum of the crystal using the density functional perturbation theory (DFPT) within the linear response method implemented in VASP with the PBE functional. It is given by the following formula

$$\varepsilon_{vib} = \frac{4\pi}{V}\sum_p \frac{Z_p^2}{\upsilon_p^2} \tag{1}$$

where υ_p is the phonon frequency of mode p, V is the unit cell volume, and Z_p is the mass-weighted mode effective Born vector. The intensity I_p of IR absorbance for a given mode p is proportional to $|Z_p|^2$.

The macroscopic static dielectric constant tensor (ε_r) was then obtained from the sum of both electronic and ionic contributions as follows:

$$\varepsilon_r = \varepsilon_\infty + \varepsilon_{vib} \tag{2}$$

The effective mass tensors of photogenerated holes (m_h^*) and electrons (m_e^*) at the band edges of each material were computed on the basis of their electronic band structure obtained from PBE and HSE06 using the following equation

$$(m^*)_{ij} = \pm\hbar^2\left(\frac{\partial^2 E_n(k)}{\partial k_i k_j}\right)^{-1} \quad (i, j = x, y, z) \tag{3}$$

where i and j denote reciprocal components, and $E_n(k)$ is the k-space dispersion relation for the n-th band. The second derivatives of the energy with respect to the wave vector in the Brillouin zone were evaluated numerically using the finite difference method.[34]

The exciton binding energy (E_b) of each compound was then computed from the hydrogenic model[35] using the formula

$$E_b = \frac{\mu}{m_0\varepsilon_r^2}R_H \tag{4}$$

where R_H is the Rydberg constant of the hydrogen atom (13.6 eV), m_0 is the free electron mass, and μ is the effective reduced mass of the exciton which is given by

DOI: 10.1021/acs.jctc.5b01076
J. Chem. Theory Comput. XXXX, XXX, XXX−XXX

$$\frac{1}{\mu} = \frac{1}{m_h^*} + \frac{1}{m_e^*} \quad (5)$$

For the cubic structures, the effective masses of the electron and the hole were taken as the arithmetic mean of the components in the three crystallographic directions, while the geometric mean was adopted for the noncubic structures. In all types of structures, the dielectric constant was obtained from the arithmetic mean of the components in the three crystallographic directions.

3. RESULTS AND DISCUSSION

3.1. Bandgaps. The bandgap is the first fundamental property of a semiconductor for its application in a photovoltaic or a photochemical device. As mentioned in the Introduction, the optimum bandgap energy in the case of sunlight absorption for photovoltaic application is requested to be between 1.1 and 1.4 eV for a simple p−n junction.[6] This zone represents a compromise between a high photocurrent in the solar cells obtained by diminishing the gap and a high photovoltage obtained by increasing the gap.

We have computed the bandgaps of a series of selected semiconductors extensively used in inorganic photovoltaic and quantum dots-sensitized solar cells such as Si, Ge, CdS, CdSe, CdTe, and GaAs crystals using the PBE and HSE06 exchange-correlation functionals. Table 2 reports the obtained values as well as the corresponding experimental ones. Our predicted bandgap values with HSE06 show an excellent agreement with the experimental data with small percentage errors in the 3−18% range, while those computed with PBE reveal strongly underestimated values by 35−71% with respect to the experimental ones. As we can see in Table 2, the calculated bandgap of 0.75 eV for Si with PBE became 1.23 eV with HSE06 which is very close to the experimental one (1.17 eV). For CdS, the computed bandgap of 1.33 eV with PBE was found 2.57 eV with HSE06 as very similarly obtained in the experiment (2.48 eV). In the case of CdTe, the calculated bandgap of 0.92 eV with PBE was significantly improved with HSE06 to give 1.56 eV which is in significant agreement with the experimental value (1.50 eV). The same behaviors were also obtained using other semiconductors such as Ge, CdSe, and GaAs, as shown in Table 2. As was already reported in theoretical studies on reference materials,[15−24,36−39] the well-known limitation of GGA functionals (commonly underestimated bandgaps) can be greatly improved by the use of HSE06. The PBE functional always gives a lower bandgap than the experimental one, while the global hybrid functional such as PBE0 and B3LYP always compute higher bandgaps than the experimental references. These results confirm once again the crucial need for using the range-separated hybrid HSE06 exchange-correlation functional rather than the standard one like PBE to accurately predict the experimental bandgaps of semiconductor compounds.

Table 2. Bandgaps (in eV) of Si, Ge, CdS, CdSe, CdTe, and GaAs Crystals Computed Using PBE and HSE06 Functionals[a]

solid	structure	PBE	HSE06	expt
Si	diamond	0.75 (35%)	1.23 (4%)	1.17[7]
Ge	diamond	0.21 (71%)	0.91 (18%)	0.74[7]
CdS	wurtzite	1.33 (46%)	2.57 (3%)	2.48[7]
CdSe	wurtzite	0.93 (46%)	1.57 (9%)	1.73[7]
CdTe	zincblende	0.92 (38%)	1.56 (3%)	1.50[7]
GaAs	zincblende	0.71 (53%)	1.68 (9%)	1.52[13]

[a]The percentage errors given in brackets are compared to experimental data.[7,13]

3.2. Dielectric Constants. The dielectric constant represents the ability of a dielectric material to screen the external electric field by the apparition of a polarization. Two contributions are present in the dielectric constant, the electronic one which is linked to the polarization originated from the reorganization of the electronic density and the vibrational one which involves the ionic motion. Previous experimental works on frequently encountered semiconductors in photovoltaic devices showed that a value greater than 10 for the static (electronic and ionic contributions) dielectric constant is enough to obtain good exciton dissociation into free charge carriers.[7,8]

We have calculated the optical (ε_∞) and static (ε_r) dielectric constant tensors of Si, Ge, CdS, CdSe, CdTe, and GaAs crystals using the PBE and HSE06 exchange-correlation functionals following the methodology described in Computational Methods given in section 2. Table 3 summarizes the obtained components in the transverse and longitudinal crystallographic directions together with the available experimental data. For ε_∞, our calculated values with HSE06 correctly reproduce the experimental data with small percentage errors going from 0 up to 12%, while those obtained with PBE give overestimated values by 5−37% compared to the experimental ones. For ε_r, similar trends revealing an excellent agreement with the

Table 3. Optical (ε_∞) and Static (ε_r) Dielectric Constants of Si, Ge, CdS, CdSe, CdTe, and GaAs Crystals Computed Using PBE and HSE06 Functionals[a]

	ε_∞			ε_r		
solid	PBE	HSE06	expt	PBE	HSE06	expt
Si	12.8 (5%)	11.8 (2%)	12.1[7]	12.8 (5%)	11.8 (2%)	12.1[7]
Ge	20.8 (20%)	16.5 (0%)	16−16.5[7]	20.8 (20%)	16.5 (0%)	16−16.5[7]
CdS	6.8 (22%)	5.3 (0%)	5.3 (⊥)[8]	10.3 (19%)	8.8 (5%)	8.3 (⊥)[7]
	6.9 (23%)	5.3 (0%)	5.3 (∥)[8]	10.8 (19%)	9.2 (5%)	8.7 (∥)[7]
CdSe	6.8 (11%)	6.2 (3%)	6.0 (⊥)[8]	9.7 (6%)	9.1 (0%)	9.1 (⊥)[7]
	7.1 (15%)	6.2 (3%)	6.0 (∥)[8]	10.2 (8%)	9.3 (0%)	9.3 (∥)[7]
CdTe	8.7 (18%)	7.4 (4%)	7.1[8]	11.7 (11%)	10.4 (0%)	10.4[7]
GaAs	17.2 (37%)	12.3 (12%)	10.8[8]	19.5 (33%)	14.6 (10%)	13.0[8]

[a]The percentage errors compared to experimental data[7,8] are given in parentheses. The symbols ⊥ and ∥ represent the transverse and longitudinal directions.

DOI: 10.1021/acs.jctc.5b01076
J. Chem. Theory Comput. XXXX, XXX, XXX−XXX

experiment data for the values computed with HSE06 (percentage errors are in the 0−10% range) and overestimation for those calculated with PBE (percentage errors compared to experimental data are in the 5−33% range) were also found. For example, if we consider Ge, the computed ε_r of 20.8 with PBE was found 16.5 with HSE06 which is very close to the experimental one (16−16.5). For CdSe, the calculated ε_r of 9.7 and 10.2 with PBE were improved by HSE06 to 9.1 and 9.3 to give exactly the same experimental values. Considering the case of CdTe, the computed ε_r of 11.7 with PBE was also corrected by HSE06 to give 10.4 as exactly obtained experimentally. Our obtained results on Si, CdS, and GaAs reported in Table 3 also show the need for going beyond the standard PBE functional and using the hybrid one like HSE06 to predict with better accuracy the experimental dielectric constants of semiconductors.

3.3. Charge Carrier Effective Masses. The effective masses of holes and electrons are the weights they seem to carry for the charge carrier transport properties of the crystal. They are related to the curvature of the valence band (for the holes) or the conduction band (for the electrons) around the extremum of the band, as it was described in Computational Methods (see section 2 for more details). The determination of the charge carrier effective masses along different crystallographic directions gives access to important information such as the possible anisotropy of charge carriers through the crystalline structure of the material. As it has been demonstrated experimentally, the effective masses of holes and electrons are both required to be smaller than $0.5m_0$ (m_0 is the free electron mass), at least in one crystallographic direction, to obtain good charge carrier transport properties.[7,13,14]

On the basis of the methodology described in Computational Methods (section 2), we have computed the effective mass tensors of the photogenerated holes (m_h^*) and electrons (m_e^*) at the band edges of Si, Ge, CdS, CdSe, CdTe, and GaAs crystals using their electronic band structures obtained from PBE and HSE06 exchange-correlation functionals. Table 4 reports the obtained values in the transverse and longitudinal crystallographic directions along with the available experimental data. Although our calculated m_h^* and m_e^* values with both PBE and HSE06 give in most of the cases a good agreement with the experimental data, those computed with HSE06 show in some cases a better accuracy with respect to the measured ones. For example, in the case of Ge, the computed m_e^* of 0.13 along the transverse direction and 0.45 along the longitudinal direction with PBE were very well corrected by HSE06 to 0.09 and 1.20 in the respective directions which are much closer to the experimental ones (0.08 and 1.57). For CdS, the calculated m_h^* of 0.23 along the transverse direction and 2.0 along the longitudinal direction with PBE were also improved by HSE06 to 0.33 and 2.42 in the respective directions to give better agreement with the experimental data (0.7 and 5). Similar trends were also obtained for the other materials such as Si, CdSe, CdTe, and GaAs, as displayed in Table 4. This clearly confirms the necessity for going beyond the standard PBE functional and using the hybrid one like HSE06 to predict with better accuracy the experimental charge carrier effective masses of semiconducting compounds.

Table 4. Effective Masses of Holes (m_h^*) and Electrons (m_e^*) of Si, Ge, CdS, CdSe, CdTe, and GaAs Crystals Computed Using PBE and HSE06 Functionals[a]

	m_h^*/m_0			m_e^*/m_0		
solid	PBE	HSE06	expt	PBE	HSE06	expt
Si	0.37	0.38	0.54 (h)[7]	0.11	0.21	0.19 (⊥)[7]
	0.08	0.11	0.15 (l)[7]	0.79	0.85	0.92 (∥)[7]
Ge	0.07	0.07	0.04 (⊥)[7]	0.13	0.09	0.08 (⊥)[7]
	0.22	0.34	0.28 (∥)[7]	0.45	1.20	1.57 (∥)[7]
CdS	0.23	0.33	0.7 (⊥)[7]	0.15	0.21	0.25[7]
	2.0	2.42	5 (∥)[7]			
CdSe	0.19	0.29	0.45 (⊥)[7]	0.08	0.09	0.11[7]
	1.7	2.12	>1 (∥)[7]			
CdTe	0.17	0.13	0.12 (l)[7]	0.08	0.1	0.09[7]
	0.78	0.82	0.81 (h)[7]			
GaAs	0.4	0.5	0.55 (h)[14]	0.09	0.08	0.07[13]
	0.12	0.09	0.08 (l)[14]			

[a] m_0 is the free electron mass. The calculated values are compared to experimental data.[7,13,14] The symbols ⊥ and ∥ mean the transverse and longitudinal directions, respectively, while (h) and (l) mean heavy and light holes.

3.4. Exciton Binding Energy. As mentioned in the Introduction, the binding energy of the exciton should be lower than the thermal energy (25 meV at room temperature) to achieve an efficient dissociation of this photogenerated exciton into free charge carriers.[9−12] Experimentally, the exciton generation is faster than atomic motions in the crystal. This is the vertical transition principle. It means that the charge-screening felt by the exciton when it is generated only comes from ε_∞ since only the electronic density can reorganize at this time scale. This is the unrelaxed exciton. Then the atoms move to adapt to the exciton. At that time, the charge screening will be governed by ε_r, giving the relaxed exciton. In the present study, it is assumed that for photovoltaic devices, the time scale of the exciton dissociation is higher than the atomic motions, and, consequently, E_b corresponds to the binding energy of the relaxed exciton.

We have calculated the exciton binding energy (E_b) of Si, Ge, CdS, CdSe, CdTe, and GaAs crystals using the hydrogenic model (see Computational Methods in section 2 for more details) along with both the PBE and HSE06 functionals. Table 5 shows the obtained values as well as the corresponding experimental data. Our computed values with HSE06 reveal an excellent agreement with the experimental data with relatively small percentage errors going from 0 up to 20%, whereas those calculated with PBE give strongly underestimated values by 12−56% compared to the experimental ones. For example, in the case of Si, the calculated E_b of 13.2 with PBE was found 15.6 with HSE06 as similarly obtained in the experiment (15).

Table 5. Exciton Binding Energy (in meV) of Si, Ge, CdS, CdSe, CdTe, and GaAs Crystals Computed Using PBE and HSE06 Functionals[a]

solid	structure	PBE	HSE06	expt
Si	diamond	13.2 (12%)	15.6 (3%)	15[9]
Ge	diamond	2.8 (30%)	5.0 (20%)	4[9]
CdS	wurtzite	15 (44%)	28.5 (5%)	27[10]
CdSe	wurtzite	9.6 (36%)	12.8 (13%)	15[9]
CdTe	zincblende	7 (30%)	10 (0%)	10[11]
GaAs	zincblende	2.2 (56%)	4.4 (12%)	5[12]

[a] The percentage errors given in brackets are compared to experimental data.[9−12]

DOI: 10.1021/acs.jctc.5b01076
J. Chem. Theory Comput. XXXX, XXX, XXX−XXX

For Ge, the computed E_b of 2.8 with PBE was significantly improved by HSE06 to give 5.0 which is very close to the experimental one (4). If we consider CdTe, the calculated E_b of 7 with PBE was also significantly improved to 10 with HSE06 to give exactly the experimental value. Our obtained results on the other compounds CdS, CdSe, and GaAs also confirm this trend, as shown in Table 5. The good description of E_b in the case of HSE06 is directly dependent on the good description of the bandgaps, while the important underestimation E_b in the case of PBE is mainly due to the strongly underestimated predicted bandgap values with respect to the experimental ones. These important results clearly demonstrate that the use of the range-separated hybrid HSE06 exchange-correlation functional rather than the standard PBE one is really needed to accurately predict the experimental exciton binding energies for semiconductor materials.

4. CONCLUSIONS

The design of new semiconductor-based electronic devices with appropriate fundamental parameters related to the light absorption, photogenerated exciton dissociation ability, and charge carrier transport properties is of major importance for harvesting solar energy into electricity.

In the work presented here, we reported the results of a systematic theoretical study on essential fundamental properties for solar energy conversion of a series of selected semiconductors widely used in inorganic photovoltaic and dye-sensitized solar cells such as Si, Ge, CdS, CdSe, CdTe, and GaAs. The electronic band gaps, optical and static dielectric constant tensors, photogenerated charge carrier effective mass tensors, and exciton binding energy of these compounds were investigated in the framework of the density functional theory (DFT) along with the standard PBE and the range-separated hybrid HSE06 exchange-correlation functionals. A systematic comparison between the computed values and the available experimental data was also highlighted to confirm the accuracy of these two computational methods.

For the electronic bandgap calculations, our predicted values with HSE06 showed an excellent agreement with the experimental data within small percentage errors in the 3−18% range, while those computed with PBE revealed strongly underestimated values by 35−71% with respect to the experimental ones. Regarding the static dielectric constant calculations, our results showed an excellent agreement with the experimental data for the values computed using HSE06 with percentage errors in the 0−10% range and overestimated values by 5−33% with respect to the measured ones for those calculated using PBE. With respect to the photogenerated charge carrier effective masses, our calculations with both PBE and HSE06 functionals provided a good agreement with the experimental data along with a better accuracy for the values computed with HSE06. Concerning the exciton binding energy calculations, our computed values with HSE06 revealed an excellent agreement with the experimental data within relatively small percentage errors going from 0 up to 20%, while those calculated with PBE provided strongly underestimated values by 12−56% compared to the experimental values.

In conclusion, we have clearly shown that the computational approach based on DFT along with the range-separated hybrid HSE06 exchange-correlation functional reveals high accuracy in predicting the optoelectronic properties of semiconductors originated from precise calculations of the electronic structure. This advanced and robust first-principle quantum methodology presented here will definitely be applied to predict novel good candidate semiconductor materials for solar energy conversion applications.

AUTHOR INFORMATION

Corresponding Author

*Phone: 966.2.808.07.88. Fax: 966.2.802.12.72. E-mail: moussab.harb@kaust.edu.sa.

Notes

The authors declare no competing financial interest.

ACKNOWLEDGMENTS

This research work was supported by King Abdullah University of Science and Technology (KAUST). The author gratefully thanks the High Performance Computing department (HPC) at KAUST for the computational time attributed to this project.

REFERENCES

(1) Shah, A.; Torres, P.; Tscharner, R.; Wyrsch, N.; Keppner, H. *Science* **1999**, *285*, 692−698.
(2) Nowotny, J.; Sorrell, C.; Sheppard, L.; Bak, T. *Int. J. Hydrogen Energy* **2005**, *30*, 521−544.
(3) Osterloh, F. E. *Chem. Mater.* **2008**, *20*, 35−54.
(4) Hernández-Alonso, M. D.; Fresno, F.; Suárez, S.; Coronado, J. M. *Energy Environ. Sci.* **2009**, *2*, 1231−1257.
(5) Hagfeldt, A.; Boschloo, G.; Sun, L.; Kloo, L.; Pettersson, H. *Chem. Rev.* **2010**, *110*, 6595−6663.
(6) Lunt, R. R.; Osedach, T. P.; Brown, P. R.; Rowehl, J. A.; Bulović, V. *Adv. Mater.* **2011**, *23*, 5712−5727.
(7) Madelung, O. *Semiconductors: Data Handbook*, 3rd ed.; Springer: New York, 2004.
(8) Young, K. F.; Frederikse, H. P. R. *J. Phys. Chem. Ref. Data* **1973**, *2*, 313−409.
(9) Pelant, I.; Valenta, J. Luminescence of Excitons. In *Luminescence Spectroscopy of Semiconductors*; Oxford University Press: Oxford, U.K., 2012.
(10) Zhang, J.; Ruf, T.; Lauck, R.; Cardona, M. *Phys. Rev. B: Condens. Matter Mater. Phys.* **1998**, *57*, 9716−9722.
(11) Taguchi, T.; Shirafuji, J.; Inuishi, Y. *Phys. Status Solidi B* **1975**, *68*, 727−738.
(12) Gilleo, M. A.; Bailey, P. T.; Hill, D. E. *Phys. Rev.* **1968**, *174*, 898−905.
(13) Vurgaftman, I.; Meyer, J. R.; Ram-Mohan, L. R. *J. Appl. Phys.* **2001**, *89*, 5815−5875.
(14) Adashi, S. *GaAs and Related Materials*; World Scientific Publishing Co. Pte. Ltd.: Singapore, 1994.
(15) Harb, M.; Sautet, P.; Raybaud, P. *J. Phys. Chem. C* **2011**, *115*, 19394−19404.
(16) Harb, M.; Sautet, P.; Raybaud, P. *J. Phys. Chem. C* **2013**, *117*, 8892−8902.
(17) Harb, M. *J. Phys. Chem. C* **2013**, *117*, 12942−12948.
(18) Harb, M.; Masih, D.; Ould-Chikh, S.; Sautet, P.; Basset, J.-M.; Takanabe, K. *J. Phys. Chem. C* **2013**, *117*, 17477−17484.
(19) Harb, M. *J. Phys. Chem. C* **2013**, *117*, 25229−25235.
(20) Harb, M.; Masih, D.; Takanabe, K. *Phys. Chem. Chem. Phys.* **2014**, *16*, 18198−18204.
(21) Harb, M.; Sautet, P.; Nurlaela, E.; Raybaud, P.; Cavallo, L.; Domen, K.; Basset, J.-M.; Takanabe, K. *Phys. Chem. Chem. Phys.* **2014**, *16*, 20548−20560.
(22) Harb, M.; Cavallo, L.; Basset, J.-M. *J. Phys. Chem. C* **2014**, *118*, 20784−20790.
(23) Harb, M. *J. Phys. Chem. C* **2015**, *119*, 4565−4572.
(24) Ziani, A.; Harb, M.; Noureldine, D.; Takanabe, K. *APL Mater.* **2015**, *3*, 096101/1−096101/5.
(25) Kresse, G.; Hafner, J. *Phys. Rev. B: Condens. Matter Mater. Phys.* **1994**, *49*, 14251−14269.

DOI: 10.1021/acs.jctc.5b01076
J. Chem. Theory Comput. XXXX, XXX, XXX−XXX

(26) Kresse, G.; Furthmüller, J. *Phys. Rev. B: Condens. Matter Mater. Phys.* **1996**, *54*, 11169−11186.
(27) Kresse, G.; Furthmüller, J. *Comput. Mater. Sci.* **1996**, *6*, 15−50.
(28) Kresse, G.; Joubert, D. *Phys. Rev. B: Condens. Matter Mater. Phys.* **1999**, *59*, 1758−1775.
(29) Blöchl, P. E. *Phys. Rev. B: Condens. Matter Mater. Phys.* **1994**, *50*, 17953−17979.
(30) Perdew, J. P.; Burke, K.; Ernzerhof, M. *Phys. Rev. Lett.* **1996**, *77*, 3865−3868.
(31) Heyd, J.; Scuseria, G. E.; Ernzerhof, M. *J. Chem. Phys.* **2003**, *118*, 8207−8215.
(32) Monkhorst, H. J.; Pack, J. D. *Phys. Rev. B* **1976**, *13*, 5188−5192.
(33) Souza, I.; Iniguez, J.; Vanderbilt, D. *Phys. Rev. Lett.* **2002**, *89*, 117602/1−117602/4.
(34) Fonari, A.; Sutton, C. *Effective Mass Calculator for Semiconductors*. http://afonari.com/emc/ (accessed November 03, 2015).
(35) Rodina, A.; Dietrich, M.; Göldner, A.; Eckey, L.; Hoffmann, A.; Efros, A.; Rosen, M.; Meyer, B. *Phys. Rev. B: Condens. Matter Mater. Phys.* **2001**, *64*, 115204/1−115204/19.
(36) Paier, J.; Marsman, M.; Hummer, K.; Kresse, G.; Gerber, I. C.; Ángyán, J. G. *J. Chem. Phys.* **2006**, *124*, 154709/1−154709/13.
(37) Paier, J.; Marsman, M.; Hummer, K.; Kresse, G.; Gerber, I. C.; Ángyán, J. G. *J. Chem. Phys.* **2006**, *125*, 249901/1−249901/2.
(38) Paier, J.; Marsman, M.; Hummer, K.; Kresse, G. *Phys. Rev. B: Condens. Matter Mater. Phys.* **2008**, *78*, 121201/1−121201/4.
(39) Henderson, T. M.; Paier, J.; Suseria, G. E. *Phys. Status Solidi B* **2011**, *248*, 767−774.

DOI: 10.1021/acs.jctc.5b01076
J. Chem. Theory Comput. XXXX, XXX, XXX−XXX